Pergamon

Int. J. Multiphase Flow Vol. 24, No. 2, pp. 225–242, 1998
© 1998 Elsevier Science Ltd. All rights reserved
Printed in Great Britain
PII: S0301-9322(97)00038-4
0301-9322/98 $19.00 + 0.00

FLOW OF CONCENTRATED NON-NEWTONIAN SLURRIES: 1. FRICTION LOSSES IN LAMINAR, TURBULENT AND TRANSITION FLOW THROUGH STRAIGHT PIPE

R. M. TURIAN†, T.-W. MA‡, F.-L. G. HSU§ and D.-J. SUNG¶

Department of Chemical Engineering, 810 S. Clinton Street, University of Illinois at Chicago, Chicago, IL 60607, U.S.A.

(Received 22 August 1996; in revised form 15 May 1997)

Abstract—Friction factor–Reynolds number correlations were established for the laminar and turbulent pipe flows of non-Newtonian slurries, and rheological model specific equations for delineating laminar–turbulent transition were derived. The correlations are based on extensive experimental data on the flow of concentrated slurries of laterite and gypsum through capillary tubes and also straight pipe test sections in a slurry pipeline flow facility. The capillary tube diameters ranged from 0.103 to 0.400 cm, and the test pipe diameters were 1.25, 2.5 and 5.0 cm (standard 1/2, 1 and 2 in pipe). For laminar flow the friction factor–Reynolds number relationship appropriate to the three-parameter Sisko model was derived, as rheometric measurements had established that this empirical rheological model did the best job of describing the shear stress–shear rate dependence for the test slurries, at all concentrations, over the whole measured range of shear rates; from about 1 to 25,200 s^{-1}. For the turbulent regime it is established that the Blasius, inverse (1/4)th power friction factor–Reynolds number form is appropriate, with Reynolds number defined in terms of the high-shear limiting viscosity η_∞ and the density of the suspension. These friction loss correlations are significant because the Sisko model, which combines a lower shear power-law region with a high-shear Newtonian asymptote, coincides with the observed shear stress–shear rate behavior of most highly-loaded fine particulate slurries over precisely the range of shear appropriate to pipeline transport. © 1998 Elsevier Science Ltd. All rights reserved

Key Words: non-Newtonian suspensions, straight pipe flow, friction factor, laminar, turbulent, laminar–turbulent transition

1. INTRODUCTION

The principal results presented here include friction factor–Reynolds number correlations for the laminar as well as turbulent flow regimes for non-Newtonian slurries obeying the Sisko model, and rheological model-specific equations for estimating laminar–turbulent transition. The friction factor–Reynolds number correlation for the laminar regime is based on solution of the flow for the Sisko fluid, and involves an appropriately modified Reynolds number, which reduces to the standard form in the Newtonian limit. In the turbulent regime it is found that the Blasius, inverse (1/4)th power friction factor relation using a Reynolds number based on the infinite-shear viscosity does a good job of predicting friction loss. New equations are derived for predicting laminar–turbulent transition for the flow in straight pipes of non-Newtonian slurries obeying the power-law and the Sisko models. In the latter case the relationship is implicit, and procedures for carrying out calculations of the transition Reynolds number, including explicit asymptotic forms of the relationships, are derived.

†To whom all correspondence should be addressed.
‡Present address: NOXSO Corp., Library, PA 15129, U.S.A.
§Present address: Lever Bros., Edgewater, NJ 07020, U.S.A.
¶Present address: Yeungnam University, Kyongsan 712-749, South Korea.

In laminar flow the correlation developed in this work predicts the experimentally measured friction factors by an absolute average deviation of 7%, and out of a total of 480 data points pertaining to flows through pipes ranging from a diameter 0.1 to 5.0 cm, only six data points had deviations exceeding 30%. For turbulent flow the absolute average deviation for a total of 922 data points was less than 11%, and only 35 data points had deviations exceeding 30%. These results are very important because, aside from the mineral slurries used as the basis for the current flow studies, the Sisko model evidently does a good job of describing the shear stress–shear rate dependence for many other industrially important, concentrated, fine-particulate, non-Newtonian slurries over precisely the range of shear most appropriate to flow in pipes. For example, extensive rheological measurements on concentrated coal–water slurries, containing narrow as well as broad size distributions of particles, in many different size ranges, result in flow curves which follow the Sisko model (Attal 1989; Turian *et al*. 1992). Over the range of shear applicable to pipeline flow, the flow curves for most concentrated non-Newtonian slurries are usually found to possess a power-law region covering the lower and the intermediate shear rate ranges, followed by an asymptotic approach to a high-shear Newtonian limit. Not only does the Sisko model embody these attributes and describe such behavior well, it also does so over the entire range of shear rates attainable even in the highest-shear rheometer, and with a unique set of unambiguously determined model parameter values. For, unlike other three-parameter empirical models, one of the model parameters, η_∞, is determined independently, as it is given by the high-shear asymptote of the viscosity–shear rate plot. Accordingly, the value of η_∞ used in the model stands for an intrinsic rheological property of the suspension; one which is instrument-geometry indifferent, and depends upon suspension microstructure. The remaining two model parameters, embodying the power-law part, are then determined to provide the best overall fit to the rheometric data over the whole range of shear.

1.1. *Empirical non-Newtonian models*

The experimentally determined shear stress (τ)–shear rate ($\dot{\gamma}$) data for the test slurries, using both rotational and mainly capillary rheometers, were used to fit empirical rheological models. We tested the two-parameter power-law, Bingham plastic and Casson, and the three-parameter Herschel–Bulkley and Sisko models. These are given by the following equations.

$$\text{Power-law model:} \quad \tau = \tilde{K}\dot{\gamma}^{\tilde{n}} \tag{1}$$

$$\text{Bingham plastic:} \quad \tau = \tau_\text{b} + \eta_\text{p}\dot{\gamma} \tag{2}$$

$$\text{Casson model:} \quad \tau^{1/2} = \tau_\text{c}^{1/2} + (\eta_\text{c}\dot{\gamma})^{1/2} \tag{3}$$

$$\text{Herschel–Bulkley model:} \quad \tau = \tau_\text{h} + K_\text{h}\dot{\gamma}^{n'} \tag{4}$$

$$\text{Sisko:} \quad \tau = \eta_\infty\dot{\gamma} + m\dot{\gamma}^{n}. \tag{5}$$

[2], [3] and [4] include a yield-stress parameter, τ_b, τ_c, and τ_h, respectively. However, curve-fitting shear stress–shear rate data to determine these yield-stress parameters will not, and generally does not, insure that a yield stress, as an intrinsic, instrument-geometry indifferent material property has been determined or, for that matter, exists. Such curve-fitted values must, unless otherwise confirmed, be viewed merely as model parameters. A detailed discussion of determination of yield stresses for suspensions has been given by Turian *et al*. (1992). Model-specific friction factor–Reynolds number relationships for the pipeline flow of non-Newtonian fluids following some of the above empirical models have been proposed.

1.2. *Flow of non-Newtonian fluids through straight pipe*

Friction factor–Reynolds number correlations for laminar non-Newtonian flow through straight pipes are generally based on solutions of the Navier–Stokes equations appropriate to the applicable rheological model. Such solutions abound in the literature and are summarized in standard texts

(Bird *et al*. 1960, 1987). Unlike the case of a Newtonian fluid, the viscosity of a non-Newtonian fluid varies with shear and, therefore, it is not obvious what reference viscosity is most appropriate for defining the Reynolds number. Metzner and Reed (1958) resolved this problem by defining a generalized Reynolds number, $\mathrm{Re}_{\mathrm{eff}}$, in terms of a so-called effective viscosity, η_{eff}, chosen so as to give a friction factor–Reynolds number dependence in laminar flow which is formally the same as for Newtonian fluids; one which would also reduce identically to the Newtonian form, $f = 16/\mathrm{Re}$, in the limit. Using the defining equation for the friction factor f in terms of the shear stress at the pipe wall, τ_{w}, we have

$$f = 2\tau_{\mathrm{w}}/\rho V^2 = [16(\eta_{\mathrm{eff}}/DV\rho)][\tau_{\mathrm{w}}/\eta_{\mathrm{eff}}(8V/D)] = 16\mathrm{Re}_{\mathrm{eff}} \qquad [6]$$

in which V is the average velocity in the pipe and ρ is the density of the slurry. This equation clearly suggests that the effective (or apparent) viscosity is to be taken as the ratio of wall shear stress, τ_{w}, to the apparent shear rate, $(8V/D)$:

$$\eta_{\mathrm{eff}} = \tau_{\mathrm{w}}/(8V/D). \qquad [7]$$

We note that $(8V/D)$ is the value of the shear rate at the pipe wall for a Newtonian fluid only. For laminar power-law fluid flow in a pipe, the wall shear rate is given by

$$\dot{\gamma}_{\mathrm{w}} = [(3\tilde{n} + 1)/4\tilde{n}](8V/D) \qquad [8]$$

and the corresponding shear stress is given by

$$\tau_{\mathrm{w}} = \tilde{K}[(3\tilde{n} + 1)/4\tilde{n}]^{\tilde{n}}(8V/D)^{\tilde{n}}. \qquad [9]$$

Capillary rheometer data, under laminar flow conditions, are usually presented as plots of $\log(D\Delta P/4L)$ vs $\log(8V/D)$, which are referred to as flow curves. The local value of the slope to the flow curve is defined as $n' = \mathrm{d}\log(\tau_{\mathrm{w}})/\mathrm{d}\log(8V/D)$. Over segments of the shear rate range where n' is constant (i.e. when the curve is a straight line, signifying local power-law behavior), one obtains by integration

$$\tau_{\mathrm{w}} = K'(8V/D)^{n'} \qquad [10]$$

in which the constant of integration K' is the intercept at $(8V/D) = 1$. Clearly, values of n' and K' will depend upon the segment of the flow curve being approximated. A generalized Reynolds number in terms of n' and K' is obtained using [7] and [10] as

$$\mathrm{Re}_{\mathrm{m}} = D^{n'}V^{(2-n')}\rho/[8^{(n'-1)}K']. \qquad [11]$$

Of course, n' is constant when power-law behavior prevails, in which case the relation with the model parameters from [1] are $n' = \tilde{n}$ and $K' = \tilde{K}[(3\tilde{n} + 1)/4\tilde{n}]^{\tilde{n}}$.

For the Sisko model [5], the relationship corresponding to [8] is implicit. From [5] the shear stress at the pipe wall is given by

$$\tau_{\mathrm{w}} = \eta_\infty\dot{\gamma}_{\mathrm{w}} + m\dot{\gamma}_{\mathrm{w}}^{n} = \eta_\infty\dot{\gamma}_{\mathrm{w}}[1 + m\dot{\gamma}_{\mathrm{w}}^{(n-1)}/\eta_\infty] = \eta_\infty\dot{\gamma}_{\mathrm{w}}(1 + X) \qquad [12]$$

in which $X = [m\dot{\gamma}_{\mathrm{w}}^{(n-1)}/\eta_\infty]$. The relation between shear rate at the wall, $\dot{\gamma}_{\mathrm{w}}$, and $(8V/D)$ is obtained from solution of the equations of motion for steady laminar tube flow (Bird *et al*. 1960, p. 70), and is given by

$$\dot{\gamma}_{\mathrm{w}} = (8V/D)/G(n, X). \qquad [13]$$

The function $G(n, X)$ is given in terms of n and $X = m\dot{\gamma}_{\mathrm{w}}^{(n-1)}/\eta_\infty$ by

$$G(n, X) = \left\{1 + 4\left[\left(\frac{n+2}{n+3}\right)X + \left(\frac{2n+1}{2n+2}\right)X^2 + \left(\frac{n}{3n+1}\right)X^3\right]\right\}/(1 + X)^3. \qquad [14]$$

Now [6] is used to define the generalized Reynolds number for the Sisko fluid. Thus

$$f = 2\tau_w/\rho V^2 = 16[\eta_\infty/DV\rho][\tau_w/\eta_\infty(8V/D)]$$
$$= (16/\mathrm{Re}_\infty)[\tau_w/\eta_\infty\dot{\gamma}_w G(n, X)]$$
$$= (16/\mathrm{Re}_\infty)[(1 + X)/G(n, X)] = 16/\mathrm{Re}_S \quad [15]$$

in which the expression from [12] was used, and $\mathrm{Re}_\infty = DV\rho/\eta_\infty$.

When $m = 0$ or $n = 1$, the Sisko model reduces to the Newtonian case, and $[(1 + X)/G(n, X)]$ in [15] reduces to 1. In order to use these equations one needs to calculate X for any given value of $(8V/D)$. The value of X can be determined by iterative solution of the transcendental relation given by [13]. Newton–Raphson, graphical as well as asymptotic methods of inverting [13] can be used.

The accessibility of laminar non-Newtonian pipe flow to analytical solution provides the framework for defining model-specific modified Reynolds numbers, and indeed results in the actual friction factor–Reynolds number relationship. In turbulent flow, however, no analytical solutions are available and the friction factor–Reynolds number dependence is uncertain. Empirical correlations for the friction factor–Reynolds number dependence in turbulent non-Newtonian pipe flow have been proposed by Dodge and Metzner (1959) for power-law fluids, by Hanks and Dadia (1971) for Bingham plastics, and by Round and El-Sayed (1983) for Herschel–Bulkley fluids, among others.

1.3. *Laminar–turbulent transition for non-Newtonian fluids*

The ratio of energy input to energy dissipation within a fluid element has been widely used to characterize the stability of non-Newtonian flow through straight pipes. While the value of this ratio depends upon whether it is determined at a point (local) or over the entire flow (integrated), it is usually assumed that laminar–turbulent transition occurs at the same value of the ratio for non-Newtonian fluids as it does for Newtonian fluids. For Newtonian fluids both local and integrated stability parameters pertaining to this ratio are expressed in terms of transition Reynolds numbers. However, since the definition of Reynolds number for non-Newtonian fluids is model-dependent, so are the laminar–turbulent transition criteria.

Ryan and Johnson (1959) defined the *local stability criterion* in general in terms of the velocity distribution, $u(r)$, in the pipe as follows:

$$Z = [D\rho u(-\mathrm{d}u/\mathrm{d}r)]/2\tau_w = D\rho u/[2_w/(-\mathrm{d}u/\mathrm{d}r)]. \quad [16]$$

It is clear that Z has the form of a Reynolds number with no reference to a fluid model. It vanishes at both the pipe wall and the centerline, attaining a maximum at some intermediate position. For a Newtonian fluid the laminar flow solution indicates that Z attains a maximum at the reduced radial position $r/R = 1/\sqrt{3}$, with

$$Z_{\max} = \sqrt{(4/27)}(DV\rho/\mu) = 0.3849\mathrm{Re}. \quad [17]$$

Taking the transition Reynolds number for laminar flow as $\mathrm{Re}_c = 21{,}000$ gives $Z_{\max} = 808$. Since Z is not restricted to any fluid model, we will assume that it is generally applicable, and take it to hold for all fluids.

Using [16] and [17] together with the velocity distribution $u(r)$ appropriate to the rheological model, laminar–turbulent transition criteria are derived. Such results have been obtained for the power-law by Ryan and Johnson (1959), for the Bingham plastic by Hanks (1981), and for the Casson and Herschel–Bulkley fluids by Hanks and Ricks (1974).

An alternative criterion, which according to Mishra and Tripathi (1971) does a better job than the local stability parameter particularly for non-Newtonian fluids with a yield stress, is the integrated stability parameter, given by

$$\Omega = E_m/\tau_w = \frac{1}{(\pi R^2 V)\tau_w}\int_0^R \frac{\rho u^2}{2} 2\pi u r \, \mathrm{d}r. \quad [18]$$

Evidently E_m, which is the mean kinetic energy per unit volume of fluid, does account for the stabilizing effect in plug flow. For Newtonian fluids $E_m = \rho V^2$, and for non-Newtonian fluids we let $E_m = \rho V^2 C$, with C given by

$$C = \int_0^1 \left(\frac{u}{V}\right)^3 \left(\frac{r}{R}\right) \mathrm{d}\left(\frac{r}{R}\right). \quad [19]$$

Since we require that $f = 16/\mathrm{Re}_{\mathrm{eff}}$ in laminar non-Newtonian pipe flow, and taking $\mathrm{Re}_{\mathrm{critical}} = 2100$ for Newtonian fluids when $C = 1$, we get

$$\mathrm{Re}_{\mathrm{eff\text{-}critical}} = 2100/C. \quad [20]$$

To apply [20] to different fluids, the model-specific modified Reynolds number, which obeys the relation $f = 16/\mathrm{Re}$ in laminar flow, must be used.

2. EXPERIMENTAL WORK AND FRICTION LOSS CORRELATIONS

Pressure drop–flowrate data for the flow in the straight pipe of our test slurries were taken using the test loops in our slurry pipeline facility. These were supplemented with the pressure drop–flowrate data obtained in conjunction with our rheological measurements on the slurries using the capillary tube rheometer system. Clearly, the latter data fell exclusively in the laminar flow regime. The starting point in our analysis of the straight pipeline flow data was to reduce the pipe and the corrected capillary flow data to the wall shear stress–apparent shear rate form. The results were then used to develop, and test, friction factor–Reynolds number correlations for non-Newtonian suspension flow in straight pipelines, and to establish and test criteria for predicting laminar–turbulent transition.

2.1. *Slurry pipeline flow facility and capillary rheometer*

The slurry flow facility used in our studies is a pilot pipeline having 1.25, 2.5 and 5.0 cm (standard 1/2, 1 and 2 in pipe) diameter flow loops, containing a variety of test fittings as well as straight pipe test sections, all with appropriately long entry and exit sections. The pilot pipeline had two centrifugal slurry pumps, the larger powered by a 30 HP and the smaller powered by a 10 HP speed-controlled electric motor. The pumps could be operated singly as well as in series. Flow rates in the 2.5 and 5.0 cm test loops were measured using 2.5 and 5.0 cm magnetic flowmeters, with magnetic heads installed in vertical sections of the test loop, and calibrations carried out using water and the actual slurries. Flow rates in the 1.25 cm test loop were measured using a weigh tank. Multitube differential manometers connected through solid traps, both of which were designed by us, were used to measure pressure drops as well as axial pressure profiles. A detailed description of the slurry flow test facility is given by Ma (1987).

The capillary tube rheometer, designed in our laboratory, is a thermostated apparatus capable of being fitted with a broad array of individually thermostated capillary tubes of different diameters and lengths, and equipped to operate over an extremely broad range of reservoir pressures (shear stresses), from below atmospheric pressure to 70 atm. A detailed description of the rheometer, the automatic pressure and flow-rate sensing apparatus, and the data acquisition and analysis PC has been presented by Turian *et al*. (1992).

2.2. *Rheological and flow experiments*

The shear stress–shear rate dependencies of all slurries were determined mainly with the capillary rheometer. To check on consistency, a few data points, at low shear, were taken using a Brookfield rotational viscometer. Dimensions of the capillary tubes used, made of precision-bore stainless steel tubing, are listed in table 1. Data analysis, including corrections for end and/or wall effects, was in accordance with the methods described in detail by Turian *et al*. (1992).

We attempted to fit the shear stress–shear rate data with each of the empirical non-Newtonian models given above by [1]–[5]. A concise summary of our findings is as follows: (1) The power-law model [1] was only capable of describing these flow curves over at most less than three cycles in

Table 1. Dimensions of capillary tubes and test pipes

Pipe I.D. (cm)	Material	Length/diameter ratio		Roughness (cm)
Capillary tubes				
0.103	stainless	295.8	443.7	
0.145	stainless	314.4	419.2	
0.217	stainless	281.1	421.7	
0.315	stainless	225.4	321.9	
0.400	stainless	203.1	253.9	
Test pipelines				
1.533	galvanized	139.2		0.000038
2.775	galvanized	98.8		
5.263	galvanized	57.9		
2.684	black steel	113.6		0.000795
5.157	black steel	59.1		0.001099

shear rate, for example, up to less than 100 s^{-1}. (2) The Bingham plastic model [2] was only suitable over the higher shear rate range, where high-shear limiting Newtonian behavior had been attained, and then only with purely curve-fitted values for the model parameter τ_b. (3) The Casson model [3] parameters were determined by least-squares fitting of the data over the entire range of shear for all test suspensions, resulting in relatively better fits than the power-law or Bingham plastic, albeit with purely curve-fitted values for the model parameter τ_c. (4) The Herschel–Bulkley [4] parameters were determined by a trial and error procedure, in which assumed values of the parameter τ_h were tried until logarithmic plots of $(\tau - \tau_h)$ against γ gave straight lines, which were then used to determine the remaining two model parameters. The trial procedure was tedious and the results were found to be very sensitive to the magnitude of the assumed τ_h. Indeed, of all models tested the Herschel–Bulkley was found to be the least satisfactory, because there is apparently on unambiguous way to determine parameter values for the model.

No such ambiguity exists in relation to the Sisko model. The high-shear limiting viscosity, η_∞, is an intrinsic material property as well as a model parameter. It is determined independently of the other model parameters from the asymptote at high shear rate of the shear stress–shear rate or viscosity–shear rate plot. Such plots for fine particulate *suspensions* almost invariably seem to approach limiting Newtonian behavior at high enough shear rates, usually preceded by a power-law region. In fact it was found that the Sisko model [5] did the best overall job of describing the shear stress–shear rate data over the whole shear range for all concentrations.

Table 2. Sisko model parameters for test slurries

Material	Concentration vol.%	Concentration wt.%	η_∞ (poise)	m†	n (—)
Titanium dioxide	17.3	45.3	0.0289	2.527	0.2310
	23.4	54.3	0.0423	5.912	0.1912
	30.7	63.7	0.8000	17.36	0.1450
	38.1	70.9	0.2331	63.02	0.0113
	41.7	74.0	0.3924	31.75	0.0290
Laterite	3.6	9.9	0.0145	3.965	0.2493
	5.7	15.1	0.0178	19.79	0.1723
	8.3	21.0	0.0224	55.53	0.1590
	12.7	30.0	0.0331	162.57	0.1419
Gypsum	10.7	21.8	0.0143	0.2958	0.3466
	19.5	36.1	0.0200	3.8561	0.1996
	25.2	44.0	0.023	5.6433	0.2995
	30.6	50.7	0.0346	9.6570	0.3025

†m has units of g cm^{-1} $s^{(n-2)}$.

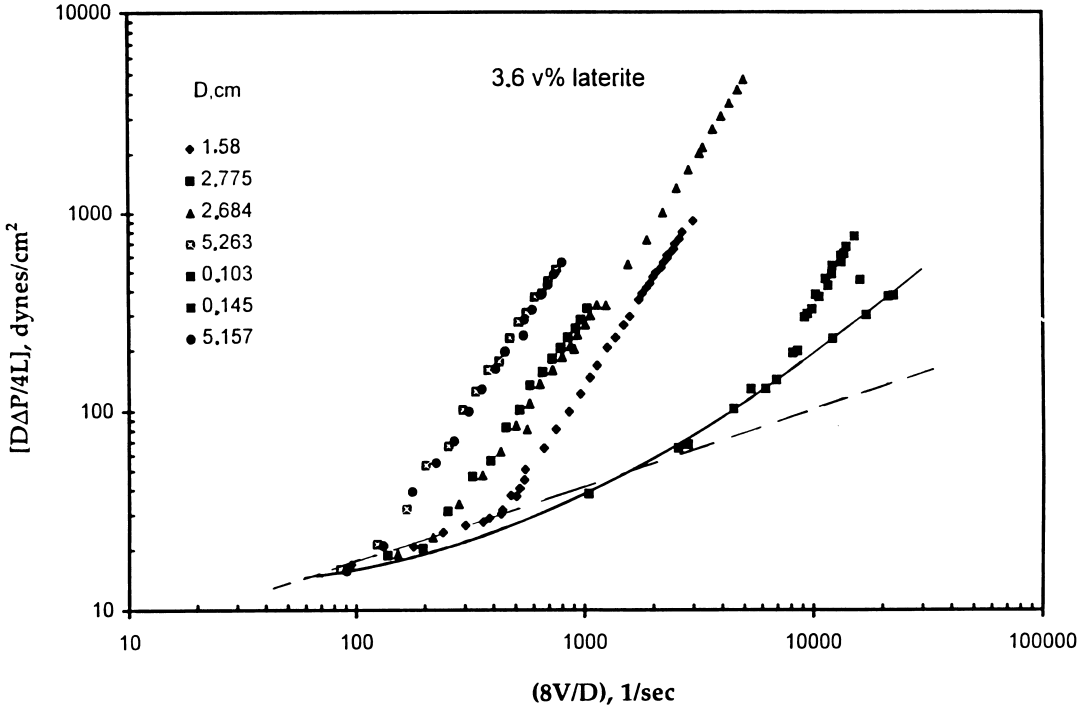

Figure 1. Flow curves ($D\Delta P/4L$) vs ($8V/D$) for 3.6 vol.% laterite suspension. Solid curve—Sisko model [5]: $\eta_\infty = 0.0145$; $m = 3.965$; $n = 0.2493$. Dashed line—[10]: $K' = 2.45$; $n' = 0.415$.

The values of the Sisko model parameters are given in table 2. With these parameter values the model predicts the shear stress–shear rate data for the test suspensions with absolute average per cent deviations of between 3.8% to a high of 12.1%. Indeed, the bulk of the data in all cases fell within a 10% band about the model curve. The solid curves in figures 6–8 represent the Sisko model fits to the data, using the parameter values given in table 2. It should be reiterated that the model parameters listed in table 2 are solely based on the shear stress–shear rate data obtained under strictly laminar flow conditions using only our capillary rheometer and the Brookfield viscometer with the rotating cylinder element.

The experiments on slurry flow through straight pipes were carried out with the temperature maintained at $25 \pm 1^{\circ}$C. Flow rates were measured using the magnetic flowmeters, which were calibrated for each concentration of the test slurry. At each pump speed setting, the data taken included the flow rate, the slurry temperature and the pressure drops over the straight pipeline test sections. In addition, for each flow rate the discharge concentration of solids was determined by collecting samples at the discharge point of the flow loop. These were used as a check on possible solids settling within the flow loop, in which case the data would have been rejected. The data were taken only after steady flowmeter and manometer readings had been established. Extensive flow experiments with water were performed to calibrate the test pipeline, to use as a reference, and to estimate wall roughness by comparison with standard friction factor–Reynolds number relationships. The water flow experiments were periodically repeated to ascertain whether changes in pipe and/or fitting characteristics had occurred as a result of particle erosion. Primary data and detailed accounts of the analyses to ascertain hydraulic diameters and establish surface roughness values are given by Ma (1987).

All the straight pipe flow data were reduced to, and plotted in, the form of $\log(D\Delta P/4L)$ vs $\log(8V/D)$, as shown in figures 1 to 8. As stated earlier, ($D\Delta P/4L$) is the actual value of the shear stress at the pipe wall, τ_w, but ($8V/D$) is the apparent shear rate, coinciding with the actual wall shear rate only in the case of Newtonian fluids. For each suspension concentration the test samples used for rheological characterization in the capillary rheometer were taken from the pipeline flow loop reservoir upon completion of the pipeline flow experiments for the given concentration. Thus

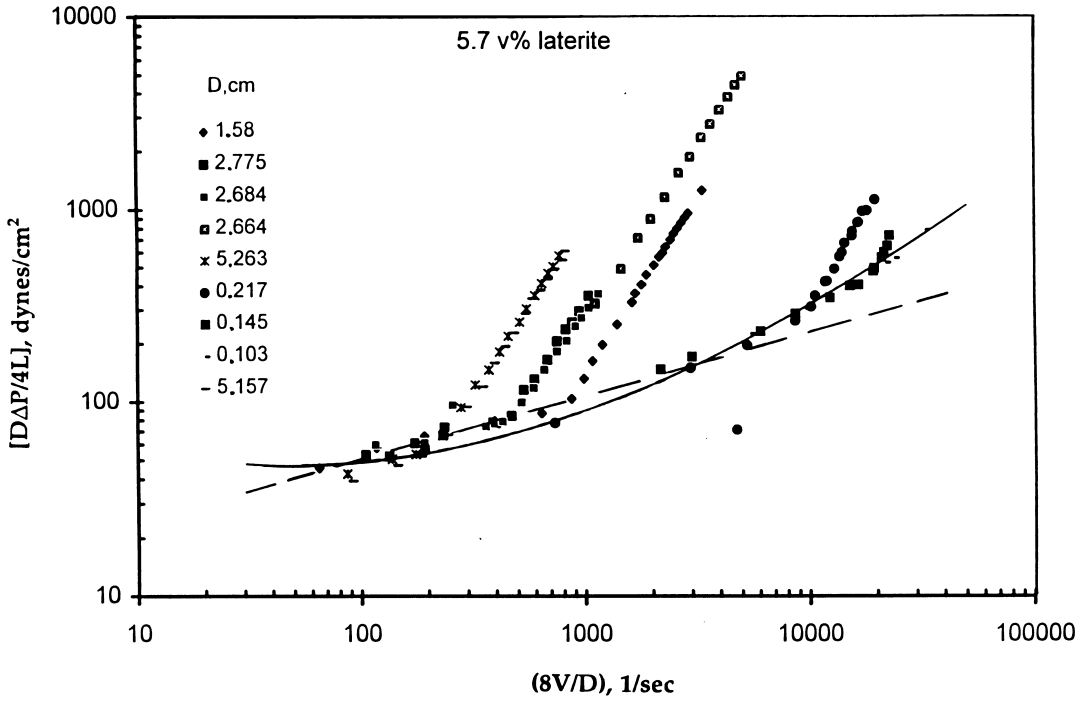

Figure 2. Flow curves ($D\Delta P/4L$) vs ($8V/D$) for 5.7 vol.% laterite suspension. Solid curve—Sisko model [5]: $\eta_\infty = 0.0178$; $m = 19.79$; $n = 0.1723$. Dashed line—[10]: $K' = 9.90$; $n' = 0.345$.

the rheological measurements were carried out on the same suspensions, which had the same preshearing history, as the suspensions in the pipeline experiments. Superposition of the pipeline and the capillary tube data in the form of the logarithmic plots of wall shear stress against apparent

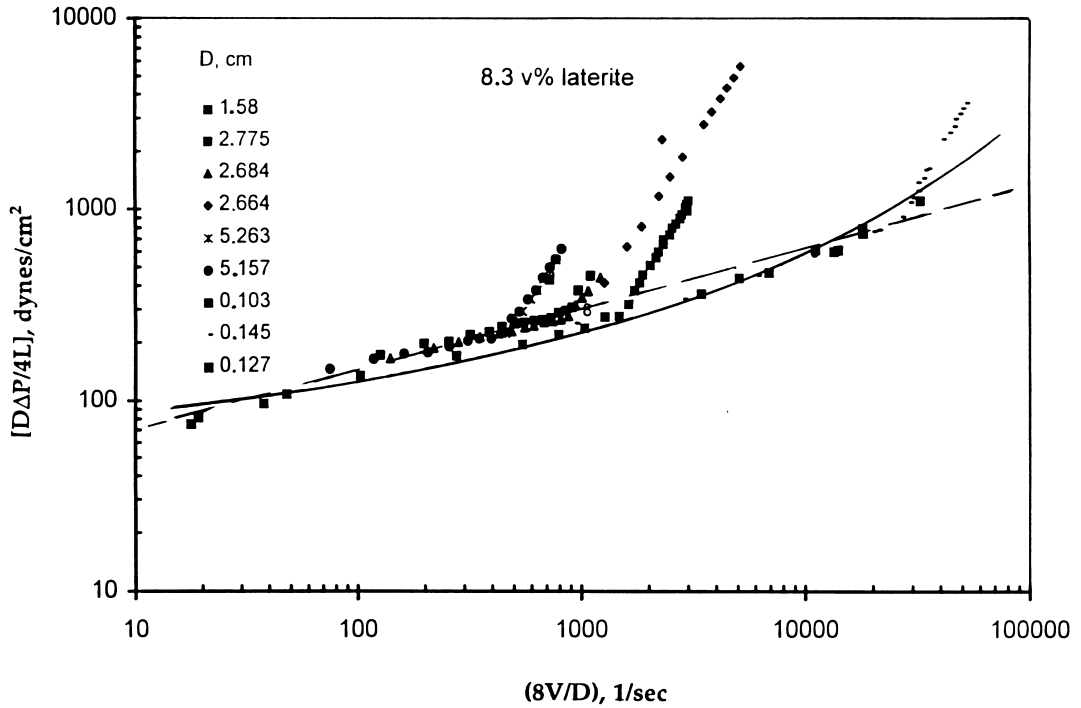

Figure 3. Flow curves ($D\Delta P/4L$) vs ($8V/D$) for 8.3 vol.% laterite suspension. Solid curve—Sisko model [5]: $\eta_\infty = 0.0224$; $m = 55.53$; $n = 0.1590$. Dashed line—[10]: $K' = 41.80$; $n' = 0.274$.

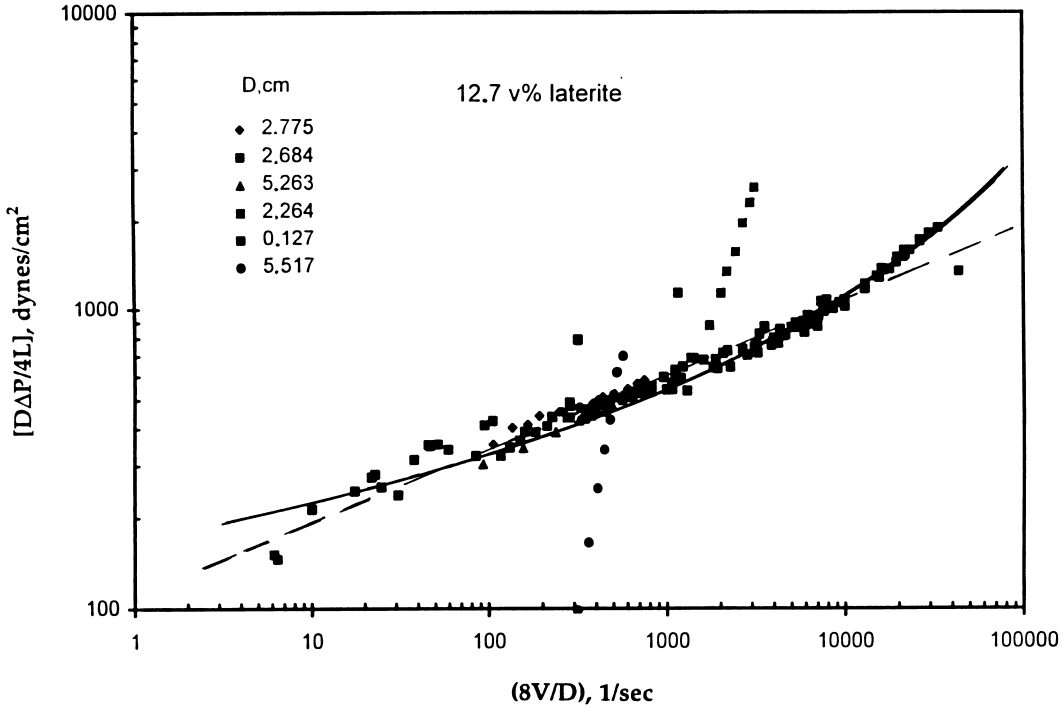

Figure 4. Flow curves ($D\Delta P/4L$) vs ($8V/D$) for 12.7 vol.% laterite suspension. Solid curve—Sisko model [5]: $\eta_\infty = 0.0331$; $m = 162.57$; $n = 0.1419$. Dashed line—[10]: $K' = 105.2$; $n' = 0.252$.

shear rate, figures 1–8, would reveal any possible discrepancies between the data from the two sources. For example, the plots in figure 3 for the 8.3% laterite and those in figure 8 for the 30.6% gypsum suspensions show some differences between the capillary tube and pipeline flow data. These differences were due to reversible rheological (thixotropy) and/or irreversible chemical (hydration, swelling) time-dependent effects.

It is clear from the plots in figures 1–8 that for each concentration the data points for laminar flow seem to define a straight line formed from the superposition of the data points for different diameters over the lower apparent shear rate range. Turbulent flow data for each diameter, on the other hand, seem to form individual, essentially parallel straight-line branches of clearly steeper slopes than the laminar flow lines. The transition from laminar to turbulent branch for each diameter seems to be smooth and marked by a fairly well-defined bend in the data plots.

Curve fits of the Sisko model to the laminar flow regions of the data are represented by the solid lines in figures 1–8. It must be emphasized that these solid lines are calculated from the Sisko model parameters determined solely on the basis of the rheological data obtained using our capillary tube rheometer and the Brookfield viscometer. To convert wall shear rates, γ_w, to the corresponding apparent shear rates, ($8V/D$), we use [13], as described earlier.

2.3. *Friction factor–Reynolds number correlations for the Sisko model*

We used the pressure drop data to establish friction factor–Reynolds number correlations for laminar as well as turbulent flow for Sisko model fluids, together with model-specific relationships for predicting laminar–turbulent transition. It was pointed out earlier that in laminar flow we use the solution to the equations of motion for steady tube flow to define a model-specific, modified Reynolds number which formally gives the same friction factor–Reynolds number dependence as for Newtonian fluids, and reduces to the Newtonian relationship in the limit. For laminar flow the friction factor–Reynolds number relationship for the Sisko fluid is taken to be the same as that given by [15], namely

$$f = (16/\mathrm{Re_S}) = (16/\mathrm{Re}_\infty)[(1 + X)/G(n, X)].$$

In order to use [15] we need to be able to determine X when the value of the apparent shear rate $(8V/D)$ is given. This is done through solution of the implicit relationship given by [13]. When we eliminate γ_w in [13] using $X = m\gamma_w^{(n-1)}/\eta_\infty$, we get

$$(m/\eta_\infty)^{1/(n-1)}(8V/D) = X^{1/(n-1)}G(n, X). \quad [21]$$

The form in [21] is suitable for direct graphical solution for X given the value of the apparent shear rate $(8V/D)$, and the rheologically determined model parameters m, n and η_∞; for example using plots of $X^{1/(n-1)}G(n, X)$ against X for various values of the Sisko model index n. Alternatively, one may use various iterative methods, e.g. Newton–Raphson, and/or available computer programs. We have used both methods, and we have also developed asymptotic forms providing explicit relationships between X and $(8V/D)$ in various limits. In using an iterative scheme, we have taken as the initial value $X = X_0$ given by

$$X_0 = m\gamma_{w0}^{(n-1)}/\eta_\infty = m[(8V/D)(3n+1)/4n]^{(n-1)}/\eta_\infty. \quad [22]$$

Reference to [8] indicates that this is the same expression for the wall shear rate as for the power-law fluid with the Sisko parameters m and n. Figure 9 depicts the comparison between [15] and the experimental friction loss data.

2.4. *Friction factor correlation for turbulent pipe flow of a Sisko fluid*

Continuing with the Sisko model as a consistent framework for correlating friction losses for the flow of non-Newtonian slurries through straight pipes, we attempted to correlate our turbulent flow data using the form $f = f(\mathrm{Re}_\infty)$. Plots of f against Re_∞, in the turbulent regime, did confirm that the friction factors in this region were determined solely by the Reynolds number based on the high-shear limiting viscosity η_∞. Furthermore, we found the dependence to be very closely approximated by the Blasius form given by

$$f = 0.0791\mathrm{Re}_\infty^{-1/4}. \quad [23]$$

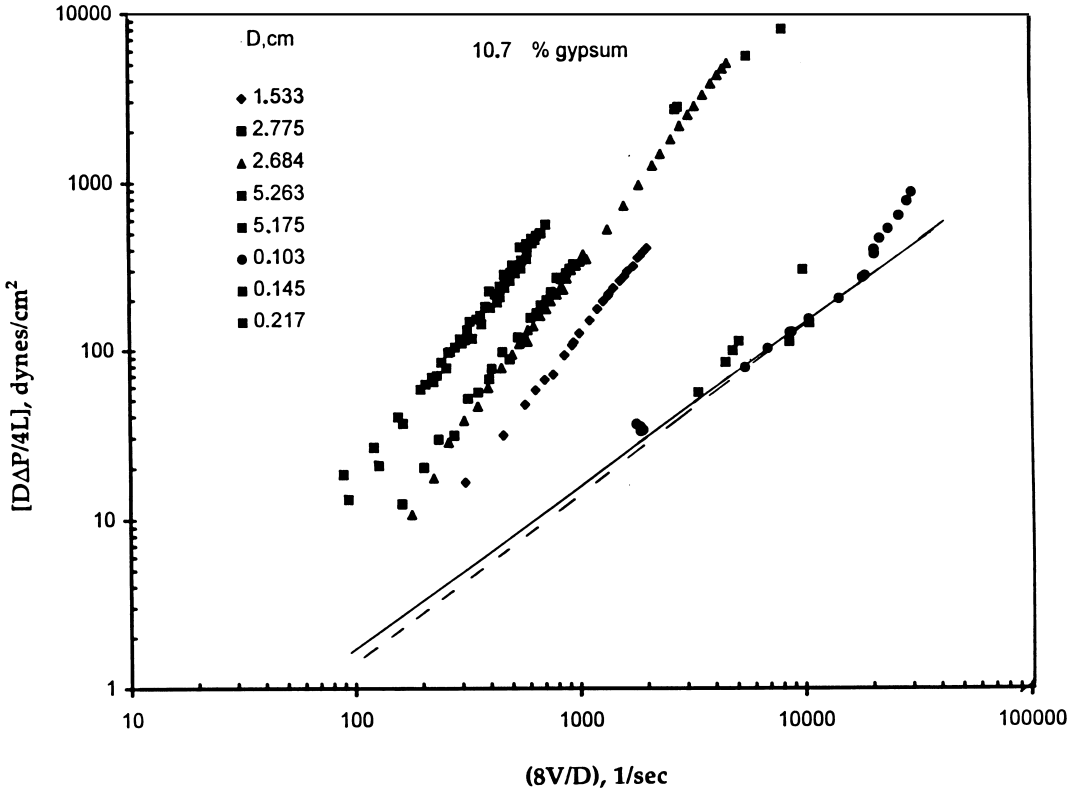

Figure 5. Flow curves $(D\Delta P/4L)$ vs $(8V/D)$ for 10.7 vol.% gypsum suspension. Solid curve—Sisko model [5]: $\eta_\infty = 0.01426$; $m = 0.2958$; $n = 0.3466$. Dashed line—[10]: $K' = 0.0185$; $n' = 0.975$.

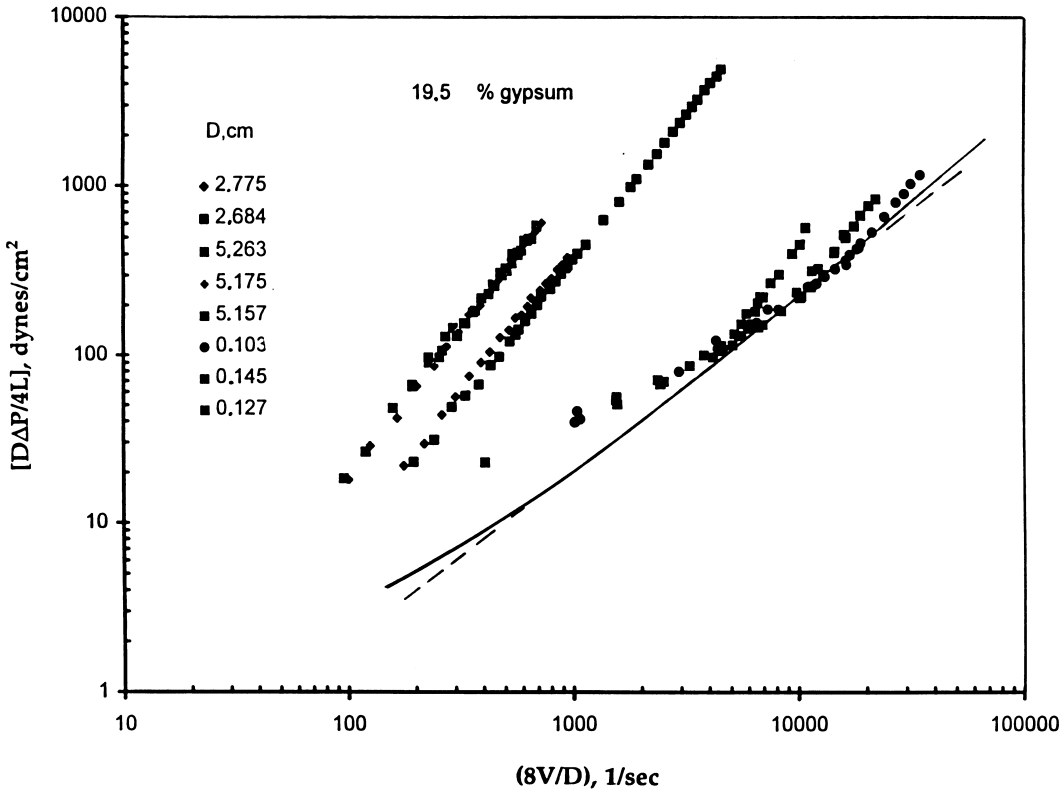

Figure 6. Flow curves ($D\Delta P/4L$) vs ($8V/D$) for 19.5 vol.% gypsum suspension. Solid curve—Sisko model [5]: $\eta_\infty = 0.020$; $m = 3.856$; $n = 0.1996$. Dashed line—[10]: $K' = 0.924$; $n' = 0.847$.

[23] is shown superimposed in figure 9 together with the experimental data for turbulent flow. The detailed comparison between experiment and [15] for laminar flow, and [23] for turbulent flow, is summarized in table 3, which also depicts the number of data points falling within various per cent deviation bands. The laminar flow data are comprised of a total of 480 points pertaining to flow through five different sizes of capillary tubes with diameters ranging from 0.103 to 0.400 cm, and also through 1.25, 2.5 and 5.0 cm diameter pipelines. The turbulent flow data consist of 922 points pertaining to flow mainly through the 1.25, 2.5 and 5.0 cm diameter pipelines.

2.5. *Laminar–turbulent transition for Sisko fluids based on local stability*

We derive laminar–turbulent transition relationships for the Sisko fluid based on both local and integrated stability criteria. To use the local stability criterion, given by [16], we first derive an

Table 3. Comparison of friction factor correlations with experiment – Sisko fluid

	Laminar flow	Turbulent flow
	[15]: $f = 16/\mathrm{Re_S}$	[23]: $f = 0.0791\ \mathrm{Re}_\infty^{-1/4}$
Total no. of data	480	922
Abs. av. % dev.	7.2	11.0
No. of data in % dev. band		
0–10%	371	498
10–20%	77	324
20–30%	26	65
>30%	6	35

%Dev. = 100 [(calc. − exp./exp.].

expression for the velocity distribution in pipe flow of a Sisko fluid. Denoting, as before, the velocity distribution by $u(r)$, and the shear rate as $\gamma = (-\mathrm{d}u/\mathrm{d}r)$, we have

$$u(r) = \int_0^u \mathrm{d}u = \int_R^r \left(\frac{\mathrm{d}u}{\mathrm{d}r}\right) \mathrm{d}r = \int_r^R \gamma \, \mathrm{d}r. \qquad [24]$$

Clearly, we assume that the no-slip condition at the pipe wall holds, i.e. $u(R) = 0$. Integrating the last integral by parts, using the result $r = (R/\tau_w)\tau$ obtained from the momentum balance on the flow (Bird *et al*. 1960), and replacing τ by its expression in terms of γ given by the Sisko model, we get

$$u(r) = R\gamma_w - r\gamma - (R/\tau_w)\int_\gamma^{\gamma_w} (\eta_\infty \gamma + m\gamma^{n+1}) \, \mathrm{d}\gamma$$

$$u(r) = R\gamma_w \left\{ 1 - (\eta_\infty \gamma_w/\tau_w)(\xi^2 - X\xi^{n+1}) - (\eta_\infty \gamma_w/\tau_w)\int_\xi^1 (\xi + X\xi^n) \, \mathrm{d}\xi \right\} \qquad [25]$$

in which $\xi = (\gamma/\gamma_w)$. We note here that the relationship between (r/R) and the reduced shear rate, ξ, used to effect the reduction from [24] to [25] is, in accordance with the Sisko model, given by

$$(r/R) = (\eta_\infty \gamma_w/\tau_w)(\xi + X\xi^n) = (\xi + X\xi^n)/(1 + X). \qquad [26]$$

When the integration in [25] is carried out, γ_w is eliminated using [13] and [14], and the quantity $(\eta_\infty \gamma_w/\tau_w)$ is replaced by $1/(1 + X)$ as indicated by [12]; we get after simplification

$$[u(r)/V] = 8[(1 + n + 2nX) - (n + 1)\xi^2 - 2nX\xi^{n+1}]/[(n + 1)(1 + X)G(n, X)]. \qquad [27]$$

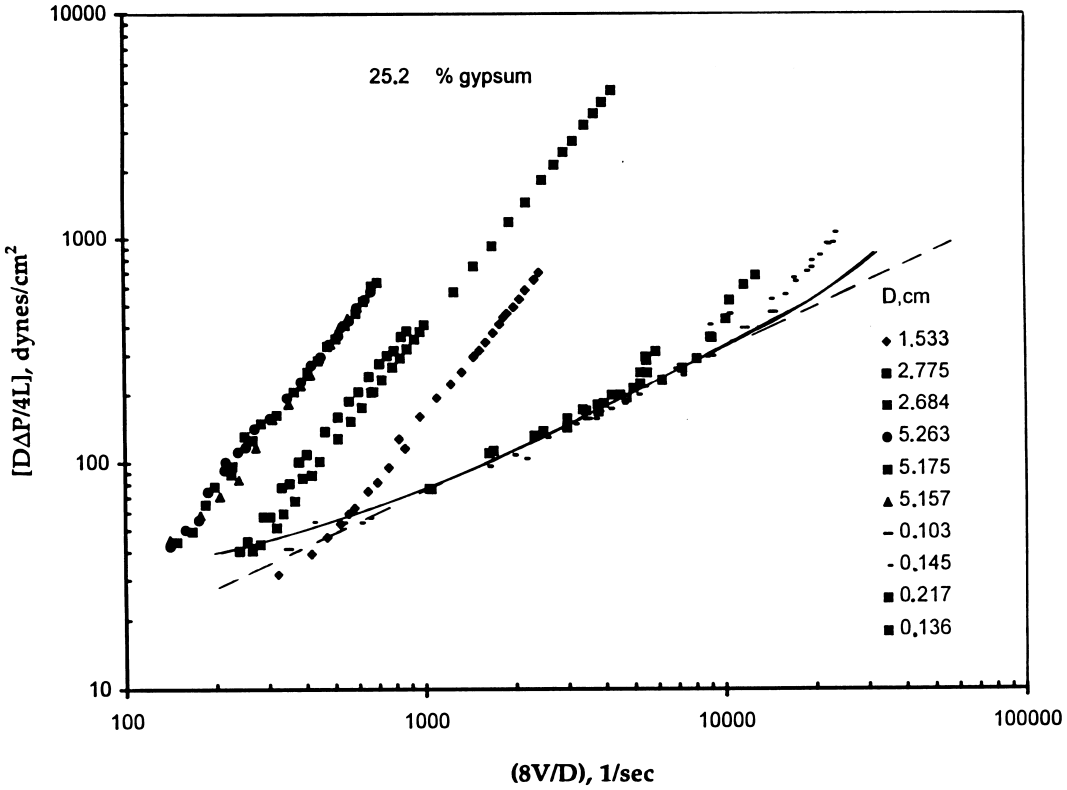

Figure 7. Flow curves $(D\Delta P/4L)$ vs $(8V/D)$ for 25.2 vol.% gypsum suspension. Solid curve—Sisko model [5]: $\eta_\infty = 0.023$; $m = 5.643$; $n = 0.2995$. Dashed line—[10]: $K' = 0.7976$; $n' = 0.654$.

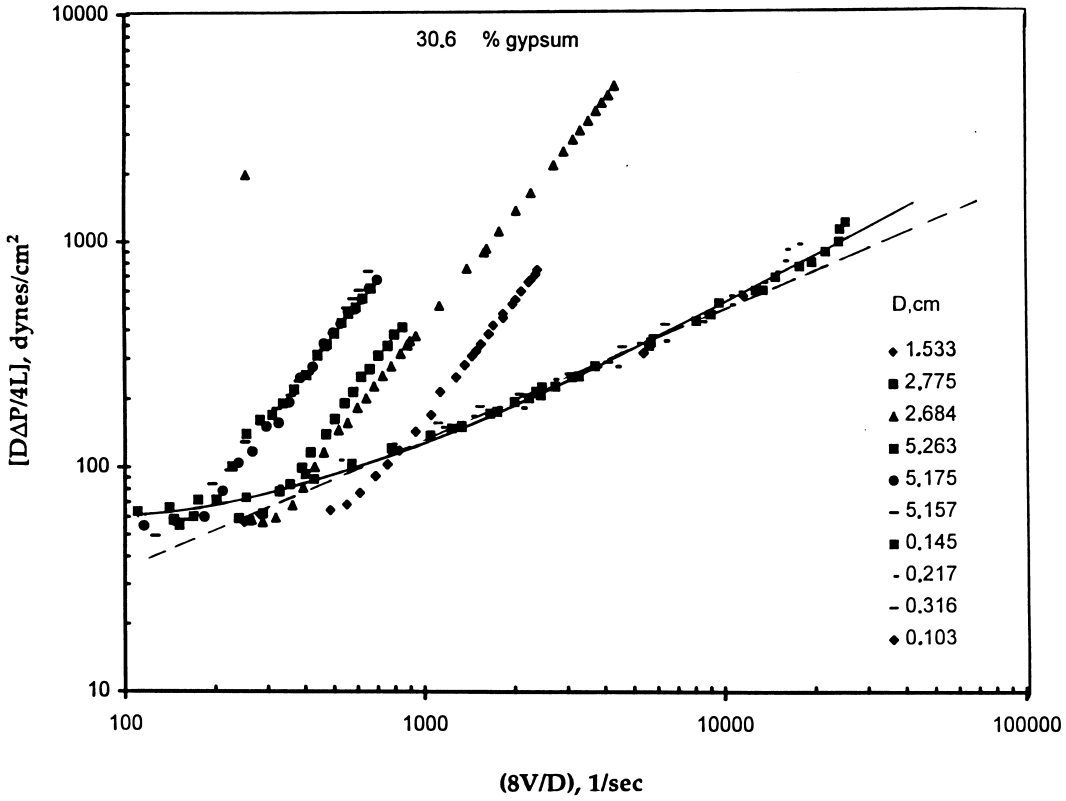

Figure 8. Flow curves ($D\Delta P/4L$) vs ($8V/D$) for 30.6 vol.% gypsum suspension. Solid curve—Sisko model [5]: $\eta_\infty = 0.0346$; $m = 9.657$; $n = 0.3025$. Dashed line—[10]: $K' = 2.453$; $n' = 0.584$.

The expression for Z in [16] for the local stability criterion can be written in terms of the variables used in the above equations as

$$Z = (1/2)(DV\rho/\eta_\infty)[u(r)/V]\xi/(1 + X). \quad [28]$$

Taking $(dZ/dr) = (dZ/d\xi)(d\xi/dr) = 0$ at transition, when $\xi = \xi_c$, we get after simplification

$$(1 + n + 2nX) - 3(n + 1)\xi_c^2 - 2n(n + 2)X\xi_c^{n+1} = 0. \quad [29]$$

[29] gives the value of $\xi = \xi_c$ when Z attains a maximum. This critical reduced shear rate value depends on n and X, and must be determined through iterative solution of [29]. Alternatively, it can be determined graphically, by preparing a plot of $X(\xi_c, n)$ against ξ_c for various values of n. This is most directly done by solving [29] for X:

$$X = [(n + 1)(\xi_c^2 - 1)]/2n[1 - (n + 2)\xi_c^{n+1}]. \quad [30]$$

[30] can now be used to express the transition in terms of the critical Reynolds number since, as reported earlier, at laminar–turbulent transition $Z_c = 808$, regardless of the rheological behavior of the fluid. This gives

$$\mathrm{Re}_{\infty c}(\mathrm{local}) = \frac{202(n + 1)(1 + X)^2 G(n, X)}{\xi_c[(1 + n + 2nX) - (n + 1)\xi_c^2 - 2nX\xi_c^{n+1}]}. \quad [31]$$

2.6. *Laminar–turbulent transition for Sisko fluids based on integral stability*

To derive the expression for the critical Reynolds number for the Sisko fluid using the integral stability criterion, we use [20] with the modified Reynolds number, $\mathrm{Re}_{s'}$. With the value $\Omega = 262.5$ corresponding to transition, we get

$$\mathrm{Re}_{\infty c}(\mathrm{integral}) = 2100I(n, X)/C = 2100(1 + X)/CG(n, X) \quad [32]$$

in which C is given by [19]. The velocity distribution given by [27] is used to determine C for the Sisko mode. Carrying out the integration and simplifying, we get

$$C = \frac{1}{(1+X)^5}\left[\frac{2}{(n+1)G(n,X)}\right]^3\left[\frac{(n+1)^3}{8} + \alpha X + \beta X^2 + \delta X^3 + \epsilon X^4 + \kappa X^5\right] \quad [33]$$

in which α, β, δ, ϵ and κ are simple polynomial functions of the Sisko model index n. These are given in Appendix A.

2.7. *Laminar–turbulent transition—comparison with experiment*

The experimental laminar–turbulent transition points were determined from the intersections of the laminar and turbulent flow curves in figures 1 to 8. These data were used to test the laminar–turbulent transition relationships developed in this work for the Sisko model. For a total number of 30 different experimentally determined laminar–turbulent transition Reynolds numbers, we found that the average absolute deviations from experiment of [31] and [32] for the Sisko model were about 25% and 20% for local and integral stability, respectively.

2.8. *Asymptotic forms of equation for wall shear rate for Sisko fluids*

We present in this section various asymptotic forms of [13] appropriate to various limits. The range of interest for n is $0 < n < 1$, and clearly $X > 0$.

Approximation for $0 < X \ll 1$.

It is convenient to let $Y = (m/\eta_\infty)(8V/D)^{(n-1)}$. Then [13] gives

$$Y = (m/\eta_\infty)(8V/D)^{(n-1)} = X[G(n,X)]^{(n-1)}. \quad [34]$$

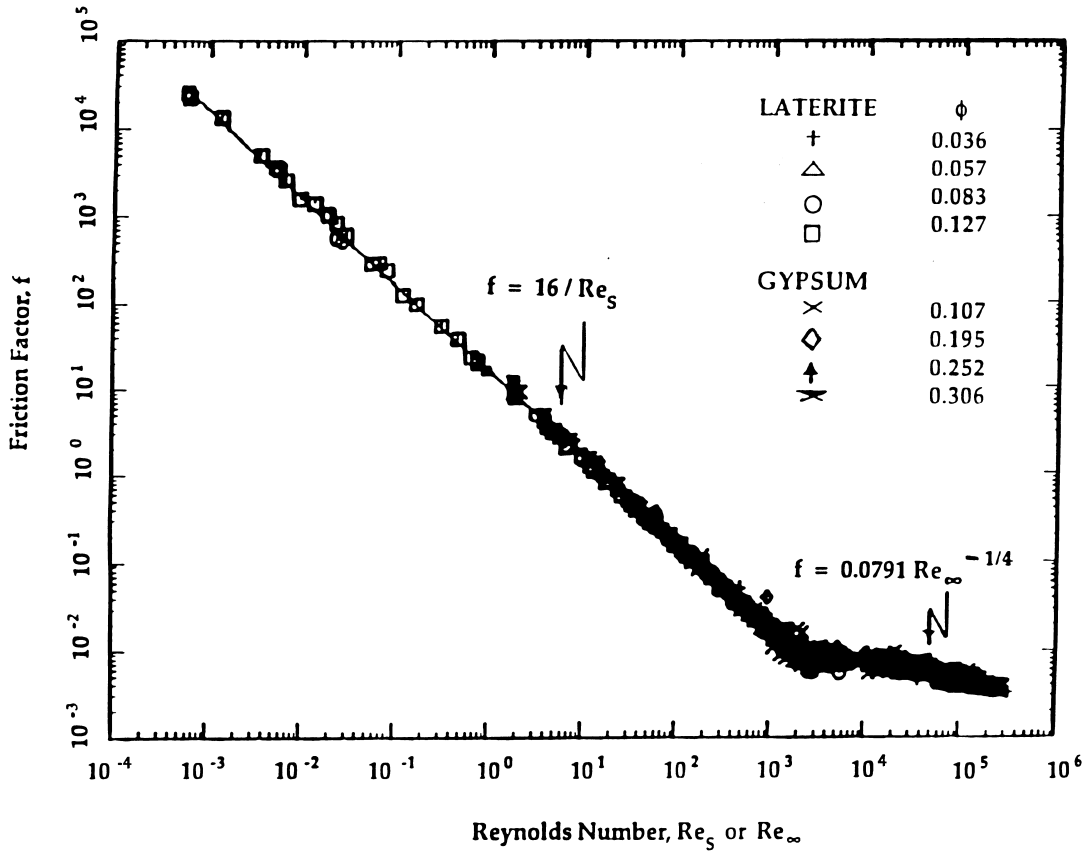

Figure 9. Friction factor–Reynolds number relationship for non-Newtonian suspension flow through straight pipe.

For $X \ll 1$ we have from [14] for $G(n, X)$

$$G(n, X) \cong (1 - 3X + 6X^2 - \ \ldots)\left[1 + 4\left(\frac{n+2}{n+3}\right)X + \left(\frac{2n+1}{2n+2}\right)X^2 + \left(\frac{n}{3n+1}\right)X^3\right]$$

$$\cong 1 + \left(\frac{n-1}{n+3}\right)X - \frac{n(n-1)}{(n+1)(n+3)}X^2 + O(X^3) \quad 0 < X \ll 1 \qquad [35]$$

and

$$Y(n, X) \cong X\left[1 + \frac{(n-1)^2}{n+3}X + O(X^2)\right] \quad 0 < X \ll 1. \qquad [36]$$

Also, the inversion of [36] gives

$$X \cong Y - \frac{(n-1)^2}{n+3}Y^2 + O(Y^3) \quad 0 < X \ll 1. \qquad [37]$$

Approximation for $X \gg 1$

For $X \gg 1$ we expand the expressions in terms of $(1/X)$. Thus we get

$$G(n, X) \cong \frac{4n}{(3n+1)} - \frac{2(n-1)}{(n+1)(3n+1)}\frac{1}{X} + O\left(\frac{1}{X^2}\right) \quad X \gg 1 \qquad [38]$$

$$Y \cong \left(\frac{4n}{3n+1}\right)^{n-1}\left[X - \frac{(n-1)^2}{2n(n+1)} + O\left(\frac{1}{X}\right)\right] \quad X \gg 1 \qquad [39]$$

and inversion of [39] gives

$$X \cong \left(\frac{3n+1}{4n}\right)^{n-1}Y + \frac{(n-1)^2}{2n(n+1)} + O\left(\frac{1}{Y}\right) \quad X \gg 1. \qquad [40]$$

Asymptotic expansions for $n \sim O(1/X) \ll 1$

The asymptotic expansions for $X \ll 1$, given by [35] to [37], are uniformly valid for all values of $0 < n < 1$. The expansions given by [38] to [40] for $X \gg 1$, however, are strictly valid for $n > O(1/X)$. The expansions fail when $nX \sim O(1)$. For $X \gg 1$ and $n \sim O(1/X) \ll 1$, we define $\zeta = nX \sim O(1)$ and we get

$$G(n, X) = \left(1 + \frac{n}{\zeta}\right)^{-3}\left[\frac{4n}{(3n+1)} + \frac{2(2n+1)}{n+1}\frac{n}{\zeta} + \frac{4(n+2)}{n+3}\left(\frac{n}{\zeta}\right)^2 + \ \cdots\right]$$

$$\cong 4n + 2\left(\frac{n}{\zeta}\right) - 2n^2\left[6 + \left(\frac{5}{\zeta}\right) + \left(\frac{5}{3}\right)\left(\frac{1}{\zeta}\right)^2\right] + \ \cdots$$

$$\cong 4n + \left(\frac{2}{X}\right) - 2n^2\left[6 + \left(\frac{5}{nX}\right) + \left(\frac{5}{3}\right)\left(\frac{1}{nX}\right)^2\right] + \ \cdots \quad n \sim O(1/X) \ll 1. \qquad [41]$$

Also, in the present case of $n \sim O(1/X) \ll 1$, it is more convenient to expand the form $Y^{1/(n-1)}$. In terms of X this is given by

$$Y^{1/(n-1)} \cong 2X^{1/(n-1)}\left[2n + \left(\frac{1}{X}\right) - n^2\left[6 + \left(\frac{5}{nX}\right) + \left(\frac{5}{3}\right)\left(\frac{1}{nX}\right)^2\right] + \ \cdots\right]. \qquad [42]$$

It is clear that [42] for $Y(X)$ provides a transcendental relationship for $X(Y)$. But it is not difficult to use, because it is valid for $n \ll 1$. We note that for $X \gg 1$ it is now possible to construct a uniformly valid *composite* approximation applicable to all n in $0 < n < 1$ by additive composition; adding the respective expansions, for example [38] and [42] for $G(n, X)$, and subtracting the common parts determined by matching the two expansions. These are not difficult to obtain, but are not given because they are necessarily transcendental by virtue of the fact that the expansions for $n \sim O(1/X) \ll 1$ were found to be so.

The precision of the foregoing asymptotic expansions depends on the value of n in $0 < n < 1$. A numerical test of these relationships yields the following results.

(1) [37], valid for $X \ll 1$, provides an excellent estimate for $X(Y)$ for all n in $0 < n < 1$. *The range of values of X* for which the expansion provides a good approximation increases as n increases. Indeed, the expansion underestimates $X(Y)$ by at most 3% for $X \leqslant 0.43$ when n is as small as 0.01. For $n = 0.9$ the range of validity of the expansion increases to such a degree that it underestimates $X(Y)$ by at most 3% for $X \leqslant 12.6$.

(2) [40], valid for $X \gg 1$, provides an approximation for $X(Y)$ when $n > O(1/X)$. For $n = 0.01$ the expansion overestimates $X(Y)$ by at most 3% for $X \geqslant 262$. However, the range of validity of the approximation increases progressively as n increases in $0 < n < 1$. For $n = 0.9$ the equation overestimates $X(Y)$ by at most 3% when $X \geqslant 0.09$.

3. CONCLUSIONS

A summary of the principal results and conclusions from this work is as follows.

The friction factor–Reynolds number correlations for the Sisko fluid developed in this work are very important because many concentrated, fine particulate, non-Newtonian slurries are describable by this relatively simple three-parameter rheological model. An important attribute of the model is that the parameters in it can be uniquely determined using rheometric data pertaining to the entire range of shear rates usually encountered in pipeline transport. This is because the mean shear rate varies in proportion to the ratio (V/D), while the Reynolds number varies with the product (VD). Accordingly, provided that small enough capillary tubes are used, laminar flow can be maintained within the capillary rheometer over shear rates for which the flow in pipelines is inevitably turbulent. Aside from suspensions, the flow curves of most non-Newtonian fluids, including solutions and melts, almost always contain regions which are power-law. The friction factor correlations developed in this work are, therefore, generally useful. The correlations for both laminar and turbulent flow regimes are capable of predicting pressure losses for non-Newtonian slurry flow in pipes with deviations comparable to those obtained from correlations or charts applicable to Newtonian fluids.

It is further noted that the correlations in this work are based on model-specific Reynolds numbers utilizing Sisko model parameters determined, independently of the pipe flow data, from rheometric measurements under strictly laminar flow conditions. Both the capillary-tube and the rotating-cylinder geometries were used in the rheometric characterizations. The model-specific Reynolds numbers are defined in terms of suspension density for both laminar and turbulent flow regimes, but whereas the generalized Reynolds number for laminar flow is derived from the steady state solution of the equations of motion applicable to the Sisko fluid, the Reynolds number for the turbulent flow regime is based only on the viscosity η_∞, a measurable material property as well as a model parameter. This suggests that the pressure loss in the turbulent flow regime for these non-Newtonian suspensions is determined mainly by the asymptotic high-shear rheological behavior of the fluid, and is then only a weak function of the fluid viscosity, as manifested by the inverse (1/4)th power Blasius dependence of friction factor on Reynolds number. It is important to note that the two factors are not inclusive. The viscosity η_∞ is a fluid property, measured, and having meaning, under laminar flow conditions, albeit in the limit of high shear. The weaker dependence of pressure loss on fluid viscosity, on the other hand, is a consequence of the increasing dominance of inertial over viscous effects which occurs under increasingly turbulent conditions. This situation, namely the dominating role of inertial effects, will be found to be even more

prominent for turbulent slurry flow through bends and fittings and other disturbances in the flow, which enhance turbulence.

The present, rheologically-based continuum approach for prediction of pressure drop for steady flow in a straight pipe is appropriate to fine particulate slurries which settle sufficiently slowly to permit meaningful rheological characterization using suitable rheometric devices. For flow through horizontal straight pipe of dense/coarse, noncolloidal, settling slurries we have previously developed a noncontinuum, multiphase flow model for prediction of pressure drop (Hsu *et al*. 1989). Comparison of pressure drops predicted using the present rheologically-based correlations with those calculated using the multiphase model approach for the gypsum slurries, which contain particles of a median size overlapping the limits of validity of the two approaches, results in excellent agreement (Hsu *et al*. 1989).

REFERENCES

Attal, J. F. (1989) Characterization, rheology and stability of coal–water mixtures. M.S. Thesis in Chemical Engineering, University of Illinois at Chicago, Chicago, IL, U.S.A.

Bird, R. B., Stewart, W. E. and Lightfoot, E. N. (1960) *Transport Phenomena*. John Wiley, New York.

Bird, R. B., Armstrong, R. C. and Hassager, O. (1987) *Dynamics of Polymeric Liquids*. *Vol*. 1: *Fluid Mechanics*. John Wiley, New York.

Dodge, D. W. and Metzner, A. B. (1959) Turbulent flow of non-Newtonian systems. *AIChE J*. **5,** 189–204.

Hanks, R. W. (1981) Laminar–turbulent transition in pipe flow of Casson model fluids. *J*. *Energy Resources Tech*., *Trans*. *ASME* **103,** 318–321.

Hanks, R. W. and Dadia, B. H. (1971) Theoretical analysis of the turbulent flow of non-Newtonian slurries in pipes. *AIChE J*. **17,** 554–557.

Hanks, R. W. and Ricks, B. L. (1974) Laminar–turbulent transition in flow of pseudoplastic fluids with yield stress. *J*. *Hydronautics* **8,** 163–166.

Hsu, F.-L., Turian, R. M. and Ma, T.-W. (1989) Flow of noncolloidal slurries in pipelines. *AIChE J*. **35,** 429–442.

Ma, T.-W. (1987) Stability, rheology and flow in pipes, bends, fittings, valves and Venturi meters of concentrated non-Newtonian suspensions. Ph.D. Thesis, University of Illinois at Chicago, Chicago, IL, U.S.A.

Metzner, A. B. and Reed, J. C. (1958) The flow of non-Newtonian fluids—correlation of laminar, transition and turbulent flow regions. *AIChE J*. **4,** 434–440.

Mishra, P. and Tripathi, G. (1971) Transition from laminar to turbulent flow of purely viscous non-Newtonian fluids in tubes. *Chem*. *Eng*. *Sci*. **26,** 915–921.

Round, G. F. and El-Sayed, E. (1983) *Proc*. 8*th Int*. *Tech*. *Conf*. *on Slurry Transport*, San Francisco, CA, pp. 15 and 111.

Ryan, N. W. and Johnson, M. M. (1959) Transition from laminar to turbulent flow in pipes. *AIChE J*. **5,** 433–435.

Turian, R. M., Hsu, F. L., Avramidis, K. S., Sung, D. J. and Allendorfer, R. K. (1992) Settling and rheology of suspensions of narrow-sized coal particles. *AIChE J*. **38,** 969–987.

APPENDIX A

The algebraic functions α, β, δ, ϵ and κ in [33] are given by the following:

$$\alpha(n) = (1 + 4n + 5n^2 + 2n^3) - [(3 + 18n + 30n^2 + 18n^3 + 3n^4)/(n + 3)] + [(3 + 24n + 42n^2 + 24n^3 + 3n^4)/(n + 5)] - [(1 + 10n + 18n^2 + 10n^3 + n^4)/(n + 7)] \quad [A1]$$

$$\beta(n) = (\tfrac{1}{2} + 3n + \tfrac{15}{2}n^2 + 5n^3) + [(15n + 57n^2 + 57n^3 + 15n^4)/2(n + 2)] - [(31n + 153n^2 + 153n^3 + 31n^4)/2(n + 3)] + [(6n + 42n^2 + 43n^3 + 6n^4)/(n + 5)] \quad [A2]$$

$$\delta(n) = (3n + 8n^2 + 9n^3) - [(12n^2 + 48n^3 + 12n^4)/(n + 3)] + [(15n^2 + 42n^3 + 15n^4)/(n + 2)] - [(18n^2 + 44n^3 + 18n^4)/(3n + 5)] + [(6n^2 + 12n^3 + 6n^4)/(3n + 1)] \quad [A3]$$

$$\epsilon(n) = (6n^2 + 7n^3) - [(24n^3 + 24n^4)/(3n + 1)] + [(6n^3 + 6n^4)/(2n + 1)] \quad [A4]$$

$$\kappa(n) = 4n^3 - [24n^4/(3n + 1)] + [12n^4/(2n + 1)] - [8n^4/(5n + 3)]. \quad [A5]$$